Efficiency Maximization of Wireless Power Transfer Based on Simultaneous Estimation of Generalized Two Parameters

Katsuhiro Hata, Takehiro Imura, and Yoichi Hori
The University of Tokyo
5-1-5, Kashiwanoha, Kashiwa, Chiba, 277-8561, Japan
Phone: +81-4-7136-3881, Fax: 81-4-7136-3881
Email: hata@hflab.k.u-tokyo.ac.jp, imura@hori.k.u-toyko.ac.jp, hori@k.u-tokyo.ac.jp

***Abstract*—A dynamic wireless power transfer (WPT) system for electric vehicles has to simplify its road-side facilities, which are installed over long distances. Although previous research has proposed secondary-side efficiency control, design constraints of the WPT system have to be imposed to obtain the reference value of the control. In this paper, an efficiency maximization method based on simultaneous estimation of the generalized two parameters, which determine the reference value of the control, is proposed. Since the generalized two parameters are estimated using secondary-side information, the design constraints of the WPT system can be eliminated. Simulations and experiments demonstrated that the estimation strategy achieved sufficient accuracy for maximum efficiency control and the proposed method drastically improved the transmitting efficiency.**

***Keywords*—Wireless power transfer, Magnetic resonance coupling, Parameter estimation, Efficiency maximization**

I. Introduction

Wireless power transfer (WPT) has gathered much attention to improve convenience and reliability of transportation applications [1]–[3]. Additionally, dynamic charging of electric vehicles (EVs) is expected to expand the limited driving distance due to the energy storage system of EVs [4], [5]. In order to implement a dynamic WPT system for EVs, it is necessary to achieve a high-power and high-efficiency transmission without dependence on the vehicle motion.

WPT via magnetic resonance coupling [6] has suitable characteristics for EV charging [2]. However, its transmitting efficiency is determined not only by magnetic coupling between a transmitter and a receiver but also by a load condition, which depends on the vehicle motion in dynamic charging. As a result, it is important to apply a control strategy for maximizing the transmitting efficiency. This paper focuses on secondary-side control to simplify the road-side facilities, which are installed over long distances in the dynamic WPT system for EVs. Although previous research has proposed an efficiency maximization method on the secondary side [7], design constraints of the WPT system has to be imposed to obtain the reference value of secondary-side efficiency control.

In this paper, an efficiency maximization method based on simultaneous estimation of the generalized two parameters, which determine the reference value of the control, is proposed. The estimation strategy is described using secondary-side information and the design constraints can be eliminated by the proposed method. The effectiveness of the proposed method is demonstrated by simulations and experiments.

II. Wireless Power Transfer System

A. System configuration

Fig. 1 shows the circuit diagram of the WPT system. The power supply consists of the DC voltage source and the full-bridge inverter. The transmitter and receiver are designed to employ a series-series (SS) compensated circuit topology of WPT via magnetic resonance coupling. The power source angular frequency ω_0 and the resonance angular frequency of the transmitter and receiver are given as follows:

$$\omega_0 = \frac{1}{\sqrt{L_1 C_1}} = \frac{1}{\sqrt{L_2 C_2}}. \tag{1}$$

Half Active Rectifier (HAR) is used as an AC-DC converter and composed of the upper arm diodes and the lower arm MOSFETs. The DC link voltage is controlled by the HAR to maximize the transmitting efficiency. The load is assumed to be a battery charging system, a motor drive system, and so on.

In order to verify the effectiveness of the proposed control strategy, the experimental equipment was implemented. The transmitter and receiver coils are shown in Fig. 2(a) and their specifications are indicated in TABLE I. The power converters, which are shown in Fig. 2(b), include the primary-side inverter and the HAR. They were controlled by a DSP (PE-PRO/F28335A, Myway) without signal communication between the primary side and the secondary side.

B. Operation modes of HAR

HAR controls the DC link voltage V_{dc} using two different operation modes, which are shown in Fig. 3.

1) Rectification mode: When the lower arm MOSFETs are turned off, HAR is operated as the diode rectifier circuit. Then, the transmitting power P flows into the DC link capacitor and increases V_{dc} if P is larger than the load power P_L.

2) Short mode: HAR short-circuits the receiver by turning on the lower arm MOSFETs. During the short mode, V_{dc} is decreased because P is cut-off and P_L is supplied from the DC link capacitor.

By switching the operation modes according to V_{dc}, HAR can control V_{dc} within the desirable range [3].

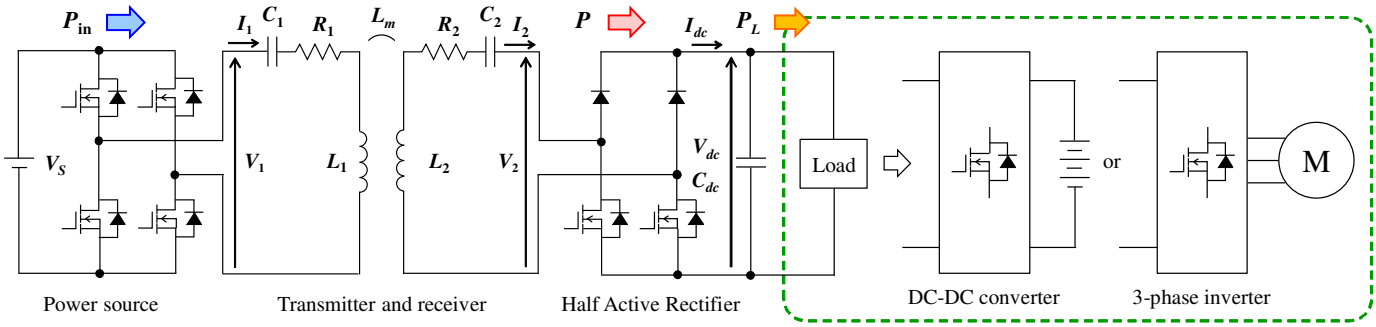

Fig. 1. Circuit diagram of the wireless power transfer system using Half Active Rectifier.

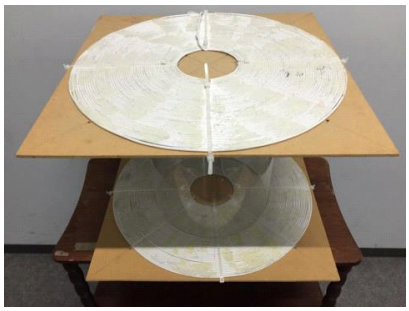

(a) Transmitter and receiver coils.

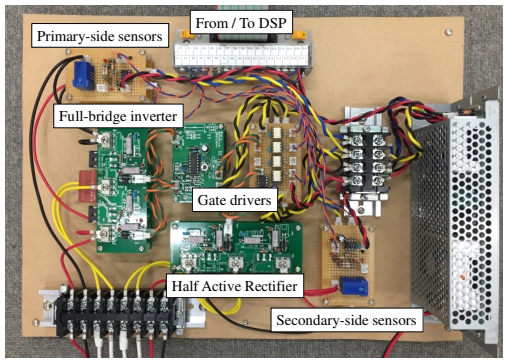

(b) Power converters.

Fig. 2. Experimental equipment.

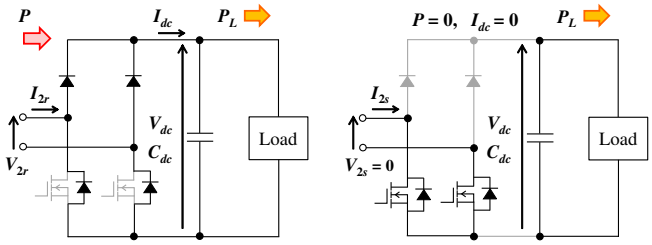

(a) Rectification mode. (b) Short mode.

Fig. 3. Operation modes of Half Active Rectifier.

TABLE I. SPECIFICATIONS OF TRANSMITTER AND RECEIVER.

	Transmitter	Receiver
Resistance R_1, R_2	1.19 Ω	1.23 Ω
Inductance L_1, L_2	617 μH	617 μH
Capacitance C_1, C_2	4000 pF	4000 pF
Resonance frequency f_1, f_2	101.3 kHz	101.3 kHz
Mutual inductance L_m	37.3 μH (Gap: 300 mm)	
	77.8 μH (Gap: 200 mm)	
Coupling coefficient k	0.060 (Gap: 300 mm)	
	0.126 (Gap: 200 mm)	
Outer diameter	440 mm	
Number of turns	50 turns	

C. Maximum efficiency control on the secondary side

Since the transmitting efficiency is determined not only by coupling between the transmitter and receiver but also by the load condition, the reference value of V_{dc} should be given properly. Although it has already been indicated using three parameters, which are unmeasurable on the secondary side [7], a simultaneous estimation method of these three parameters using secondary-side information remains unrealized. In order to eliminate the need for signal communication between the primary side and the secondary side, some parameters have to be fixed and given by design constraints of the WPT system.

In this paper, the reference value of maximum efficiency control on the secondary side is derived using the generalized two parameters, which are estimated based on secondary-side information. Additionally, a simultaneous estimation method of the generalized two parameters is described in chapter IV.

III. CIRCUIT ANALYSIS

In this chapter, the circuit analysis of the WPT system is indicated to derive the reference value of maximum efficiency control on the secondary side. Then, a resistive load and a constant voltage load are addressed.

A. Resistive load condition

Fig. 4(a) shows the equivalent circuit of WPT via magnetic resonance coupling using the resistive load [8]. In this study, iron loss is assumed to be negligible small. When the primary-side inverter generates a square voltage wave, the RMS value of the fundamental primary voltage V_{11} is expressed as follows:

$$V_{11} = \frac{2\sqrt{2}}{\pi} V_1 = \frac{2\sqrt{2}}{\pi} V_S. \tag{2}$$

Then, the voltage ratio A_V and the current ratio A_I between the primary side and the secondary side are given

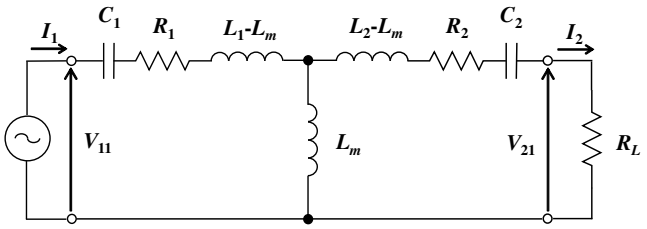

(a) Resistive load.

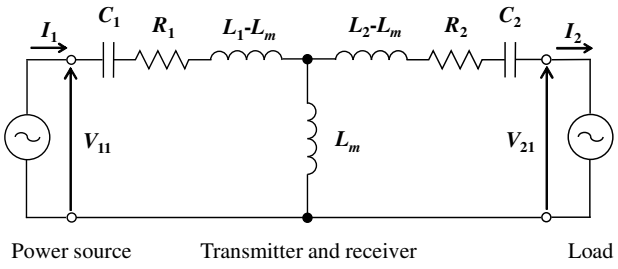

(b) Constant voltage load.

Fig. 4. Equivalent circuit of wireless power transfer via magnetic resonance coupling.

as follows:

$$A_V = \frac{V_{21}}{V_{11}} = \frac{\omega_0 L_m R_L}{R_1(R_2+R_L)+(\omega_0 L_m)^2} \tag{3}$$

$$A_I = \frac{I_2}{I_1} = \frac{\omega_0 L_m}{R_2+R_L} \tag{4}$$

where V_{21}, I_1, I_2 are the RMS values of the fundamental secondary voltage, the primary current, and the secondary current, respectively.

From eq. (3) and eq. (4), the transmitting efficiency η and the charging power P are described as follows:

$$\eta = \frac{(\omega_0 L_m)^2 R_L}{(R_2+R_L)\{R_1(R_2+R_L)+(\omega_0 L_m)^2\}} \tag{5}$$

$$P = \frac{{A_V}^2}{R_L}{V_{11}}^2 = \frac{(\omega_0 L_m)^2 R_L}{\{R_1(R_2+R_L)+(\omega_0 L_m)^2\}^2}{V_{11}}^2. \tag{6}$$

When $V_{11} = 100$ V and $L_m = 77.8$ μH, Fig. 5(a) shows R_L versus η and P. Then, the load resistance $R_{L\eta\max}$, which maximizes η, is given as follows [9]:

$$R_{L\eta\max} = \sqrt{R_2\left\{\frac{(\omega_0 L_m)^2}{R_1}+R_2\right\}}. \tag{7}$$

B. Constant voltage load condition

Since the DC link voltage V_{dc} is controlled on the secondary side, the actual load has to be assumed not as the resistive load but as the constant voltage load. The equivalent circuit of WPT via magnetic resonance coupling using the constant voltage load is shown in Fig. 4(b). Then, V_{21} has to be given both during the rectification mode and during the short mode of HAR.

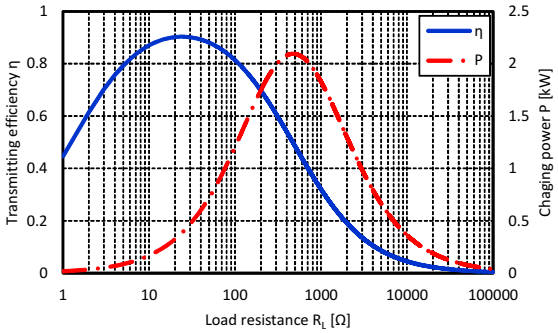

(a) Resistive load.

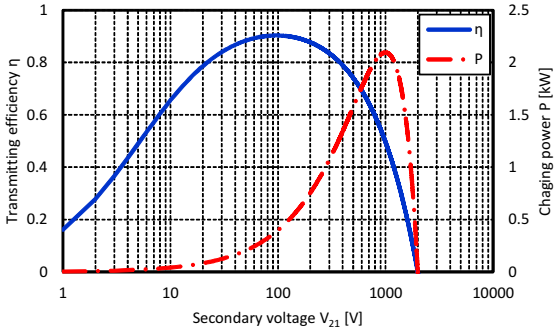

(b) Constant voltage load.

Fig. 5. Transmitting efficiency η and charging power P.

Because the rectification mode of HAR is worked as the diode rectifier, the secondary voltage is assumed to be a square wave with the same amplitude as the DC link voltage and the same frequency as the primary voltage if the voltage variation in V_{dc} is negligible small [10]. On the other hand, the secondary voltage during the short mode of HAR equals to 0 because the receiver is shorted.

When V_{21r}, V_{21s} are defined as the fundamental secondary voltage during the rectification mode and during the short mode, they are calculated as follows:

$$V_{21r} = \frac{2\sqrt{2}}{\pi}V_{2r} = \frac{2\sqrt{2}}{\pi}(V_{dc}+2V_f) \tag{8}$$

$$V_{21s} = \frac{2\sqrt{2}}{\pi}V_{2s} = 0 \tag{9}$$

where V_f is the forward voltage of the diodes.

Additionally, the phase difference between the primary voltage and the secondary voltage is assumed to be 90 degrees [10]. From the circuit equation, the secondary current I_2 is calculated as follows:

$$I_2 = \frac{\omega_0 L_m V_{11} - R_1 V_{21}}{R_1 R_2 + (\omega_0 L_m)^2}. \tag{10}$$

Then, the equivalent resistance of the constant voltage load R_L is obtained as follows:

$$R_L = \frac{V_{21}}{I_2} = \frac{\{R_1 R_2 + (\omega_0 L_m)^2\}V_{21}}{\omega_0 L_m V_{11} - R_1 V_{21}}. \tag{11}$$

Consequently, the constant voltage load can be treated equally with the resistive load as shown in Fig. 4(a).

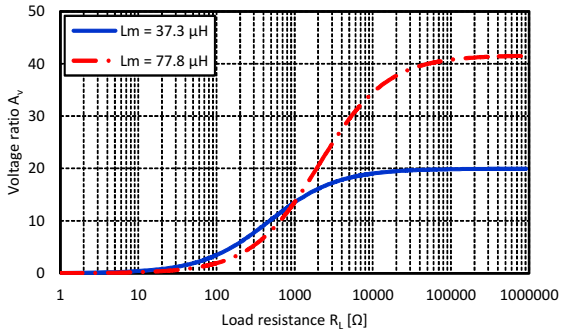

Fig. 6. Load resistance R_L vs. voltage ratio A_V.

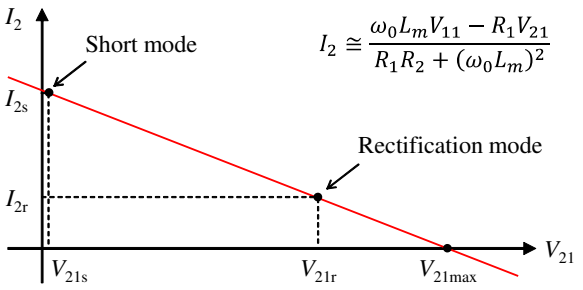

Fig. 7. Secondary current I_2 in each modes of HAR.

When $V_{11} = 100$ V and $L_m = 77.8$ μH, Fig. 5(b) shows V_{21} versus η and P. From eq. (3) and eq. (7), the fundamental secondary voltage $V_{21\eta\max}$, which maximizes η, is expressed as follows [7]:

$$V_{21\eta\max} = \sqrt{\frac{R_2}{R_1}} \frac{\omega_0 L_m}{\sqrt{R_1 R_2 + (\omega_0 L_m)^2} + \sqrt{R_1 R_2}} V_{11}. \quad (12)$$

However, eq. (12) includes the fundamental primary voltage V_{11}, the primary coil resistance R_1, and the mutual inductance between the transmitter and the receiver L_m, which are unmeasurable on the secondary side. Although previous research has proposed a simultaneous estimation method of V_{11} and L_m [11], R_1 has to be fixed and given by the design constraints of the WPT system.

C. Generalized two parameters

This paper derives $V_{21\eta\max}$ using the generalized two parameters x_1, x_2, which are defined as follows:

$$x_1 = k^2 Q_1 Q_2 = \frac{(\omega_0 L_m)^2}{R_1 R_2} \quad (13)$$

$$x_2 = V_{21\max} = \frac{\omega_0 L_m V_{11}}{R_1} \quad (14)$$

where x_1, x_2 are given to include V_{11}, R_1, and L_m. Then, x_1 implies maximum efficiency of the WPT system [2], [12] and x_2 is the fundamental value of the maximum available secondary voltage $V_{21\max}$. Fig. 5(b) shows that $V_{21\max}$ exists when P equals to 0 excluding $V_{21} \neq 0$. Then, the equivalent resistance R_L, which is given by eq. (11), becomes ∞. It is confirmed that Fig. 6 shows the voltage ratio A_V becomes saturated according to the increase in R_L. Its maximum value $A_{V\,sat}$ is described as follows [9]:

$$A_{V\,sat} = \frac{V_{21\max}}{V_{11}} = \frac{\omega_0 L_m}{R_1}. \quad (15)$$

From eq. (12), eq. (13), and eq. (14), $V_{21\eta\max}$ can be derived as follows:

$$V_{21\eta\max} = \frac{V_{21\max}}{1 + \sqrt{1 + k^2 Q_1 Q_2}} = \frac{x_2}{1 + \sqrt{1 + x_1}}. \quad (16)$$

Therefore, the reference value of maximum efficiency control can be calculated based on simultaneous estimation of x_1 and x_2 using secondary-side information without design constraints of the WPT system.

IV. Simultaneous Estimation of Generalized Two Parameters

This chapter indicates the simultaneous estimation method of x_1 and x_2 using secondary-side information. The estimation equation is derived based on the theoretical equation of the secondary current I_2. Eq. (10) is transformed as follows:

$$V_{21} + R_2 I_2 + k^2 Q_1 Q_2 R_2 I_2 = V_{21\max}. \quad (17)$$

Then, the estimation equation is obtained as follows:

$$(-R_2 I_2) x_1 + x_2 = V_{21} + R_2 I_2 \quad (18)$$

Fig. 7 shows the fundamental secondary voltage V_{21} versus the secondary current I_2 and the measurement points during the rectification mode and during the short mode. Since HAR utilize the two operation modes for secondary-side control, V_{21} and I_2 can be measured in each modes. Because V_{21r}, V_{21s} are given by eq. (8) and eq. (9), I_{2r}, I_{2s} are theoretically calculated by eq. (10). When the unknown parameter $\boldsymbol{x}$ is defined as follows:

$$\boldsymbol{x} = [x_1 \quad x_2]^T = \left[k^2 Q_1 Q_2 \quad V_{21\max}\right]^T \quad (19)$$

the estimated parameter $\hat{\boldsymbol{x}}$ is obtained as follows:

$$\hat{\boldsymbol{x}} = [\hat{x}_1 \quad \hat{x}_2]^T = \boldsymbol{A}^{-1}\boldsymbol{b} \quad (20)$$
$$\boldsymbol{A} := \begin{bmatrix} -R_2 I_{2r} & 1 \\ -R_2 I_{2s} & 1 \end{bmatrix}, \quad \boldsymbol{b} := \begin{bmatrix} V_{21r} + R_2 I_{2r} \\ V_{21s} + R_2 I_{2s} \end{bmatrix}.$$

Then, $\boldsymbol{x}$ is estimated based on secondary-side information because V_{21r}, I_{2r}, V_{21s}, and I_{2s} are the measured values during the rectification mode and during the short mode. Additionally, the secondary coil resistance R_2 is given on the secondary side.

V. Simulation and Experiment

A. Experimental condition

The circuit configuration of the experimental setup is illustrated in Fig. 1. The source voltage V_S was tuned to 10 V or 20 V and the transmitting distance was set to 200 mm or 300 mm. The DC link voltage V_{dc} was regulated by an electronic load from 2.5 V to 50 V. I_2 was measured during each modes of HAR and used for simultaneous estimation of the generalized two parameters x_1, x_2. The reference voltage of maximum efficiency control was calculated based on the estimated values $\hat{x_1}, \hat{x_1}$ and efficiency improvement with maximum efficiency control using the estimated reference voltage was verified.

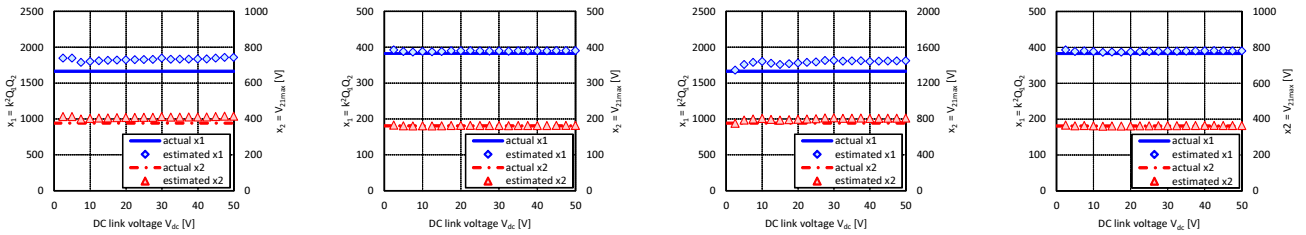

(a) $V_1 = 10$ V, $L_m = 77.8$ μH. (b) $V_1 = 10$ V, $L_m = 37.3$ μH. (c) $V_1 = 20$ V, $L_m = 77.8$ μH. (d) $V_1 = 20$ V, $L_m = 37.3$ μH.

Fig. 8. Simulation results of x_1 and x_2 estimation.

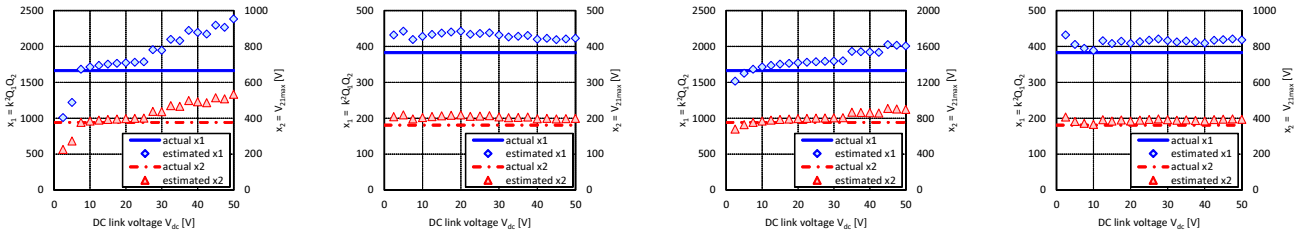

(a) $V_1 = 10$ V, $L_m = 77.8$ μH. (b) $V_1 = 10$ V, $L_m = 37.3$ μH. (c) $V_1 = 20$ V, $L_m = 77.8$ μH. (d) $V_1 = 20$ V, $L_m = 37.3$ μH.

Fig. 9. Experimental results of x_1 and x_2 estimation.

B. Simultaneous estimation of generalized parameters

The simulation results of x_1 and x_2 estimation are shown in Fig. 8. The actual values of x_1 and x_2 are represented by the lines and the estimation results $\hat{x}_1, \hat{x}_2$ are indicated by the plots. From Fig. 8(a) and Fig. 8(c), which are the large L_m condition, it is confirmed that $\hat{x}_2$ is adequately estimated but $\hat{x}_1$ is slightly larger than x_1. This is because the difference of I_2 between each operation modes of HAR is quite small. As a result, measurement capability affects the estimation accuracy. In this simulation, the measured values were rounded to 3 significant digits.

Fig. 9 shows the experimental results of x_1 and x_2 estimation. Although the estimation accuracy is reduced compared to the simulation results, it is important not to make a precise estimate of x_1 and x_2 but to obtain the reference value of the control and to maximize the transmitting efficiency. Therefore, the reference voltage calculation and efficiency maximization based on the estimation results $\hat{x}_1, \hat{x}_2$ were demonstrated.

C. Reference voltage calculation and efficiency maximization

Fig. 10 and Fig. 11 show the calculation results of the reference voltage based on $\hat{x}_1, \hat{x}_2$, which are described in Fig. 8 and Fig. 9. The calculated reference voltages are well accorded with their actual values except for Fig. 11(a). As a result, it is difficult to obtain the precise value of the reference voltage at the low power and high coupling condition.

Finally, efficiency maximization using the calculated reference voltage was verified and its results are shown in Fig. 12 and Fig. 13. If the DC link voltage is away from the optimum voltage, which maximize the transmitting efficiency η, before the control, η is drastically increased. Since efficiency degradation due to the estimation error is not confirmed, the estimation accuracy of x_1 and x_2 is sufficient and the proposed method is feasible for maximum efficiency control.

VI. Conclusion

This paper proposed an efficiency maximization method of WPT based on simultaneous estimation of the generalized two parameters, which determine a reference value of maximum efficiency control on the secondary side. The proposed method can eliminate design constraints of the WPT system for the control because the generalized two parameters and the reference value were estimated only using secondary-side information. Simulations and experiments demonstrated that estimation accuracy of the proposed method was sufficient for the control and the transmitting efficiency was much improved by the proposed method. Future works are to implement a real-time estimation and control strategy and to apply the proposed method to EV applications.

Acknowledgments

This work was partly supported by JSPS KAKENHI Grant Number 25709020, 15H02232, and 16J06942.

References

[1] G. A. Covic and J. T. Boys, "Modern trends in inductive power transfer for transportation application," *IEEE J. Emerg. Sel. Topics Power Electron.*, vol. 1, no.1, pp. 28–41, Mar. 2013.

[2] S. Li and C. C. Mi, "Wireless power transfer for electric vehicle applications," *IEEE J. Emerg. Sel. Topics Power Electron.*, vol. 3, no.1, pp. 4–17, Mar. 2015.

[3] D. Gunji, T. Imura, and H. Fujimoto, "Basic study of transmitting power control method without signal communication for wireless in-wheel motor via magnetic resonance coupling," in *Proc. IEEE/IES ICM*, 2015, pp. 313–318.

[4] S. Chopra and P. Bauer, "Driving range extension of EV with on-road contactless power transfer—a case study," *IEEE Trans. Ind. Electron.*, vol. 60, no. 1, pp. 329–338, Jul. 2013.

[5] S. Y. Choi, B. W. Gu, S. Y. Jeong, and C. T. Rim, "Advances in wireless power transfer systems for roadway-powered electric vehicles," *IEEE J. Emerg. Sel. Topics Power Electron.*, vol. 3, no.1, pp 18–36, Mar. 2015.

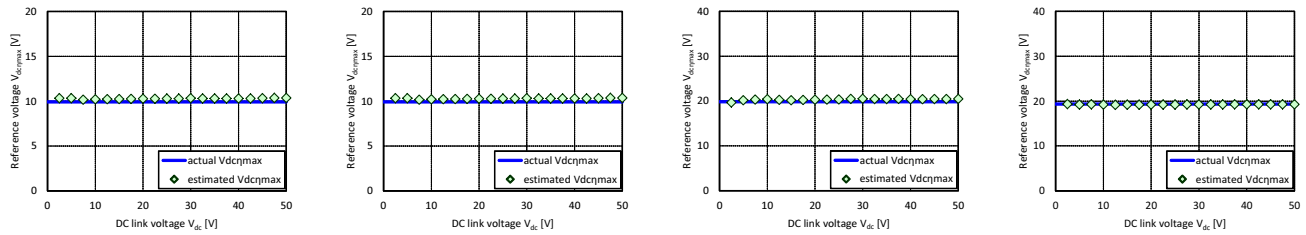

(a) $V_1 = 10$ V, $L_m = 77.8$ μH. (b) $V_1 = 10$ V, $L_m = 37.3$ μH. (c) $V_1 = 20$ V, $L_m = 77.8$ μH. (d) $V_1 = 20$ V, $L_m = 37.3$ μH.

Fig. 10. Simulation results of reference voltage calculation for efficiency maximization.

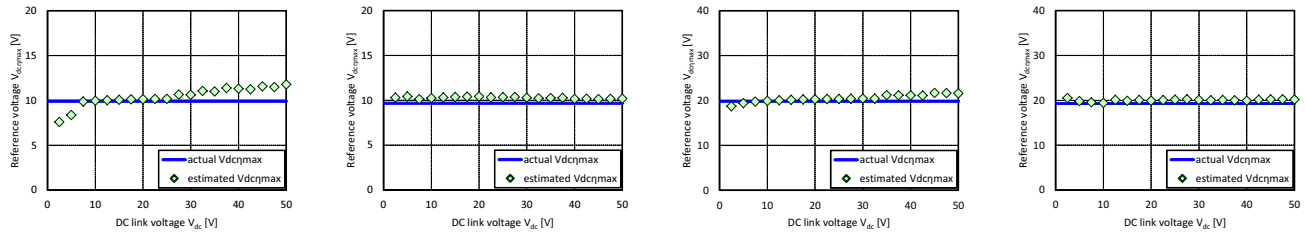

(a) $V_1 = 10$ V, $L_m = 77.8$ μH. (b) $V_1 = 10$ V, $L_m = 37.3$ μH. (c) $V_1 = 20$ V, $L_m = 77.8$ μH. (d) $V_1 = 20$ V, $L_m = 37.3$ μH.

Fig. 11. Experimental results of reference voltage calculation for efficiency maximization.

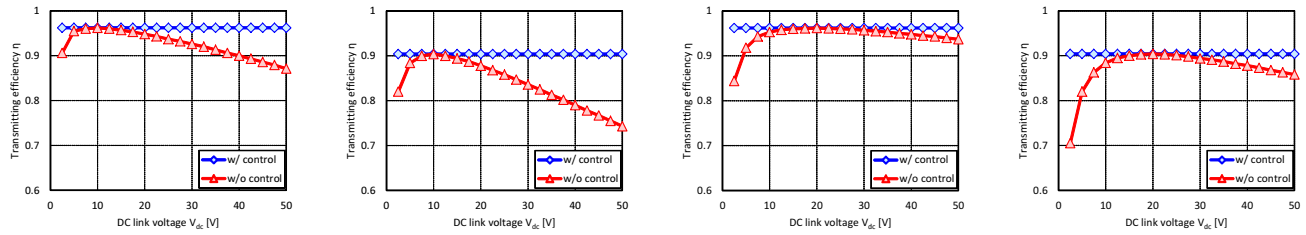

(a) $V_1 = 10$ V, $L_m = 77.8$ μH. (b) $V_1 = 10$ V, $L_m = 37.3$ μH. (c) $V_1 = 20$ V, $L_m = 77.8$ μH. (d) $V_1 = 20$ V, $L_m = 37.3$ μH.

Fig. 12. Simulation results of efficiency maximization using calculated reference voltage.

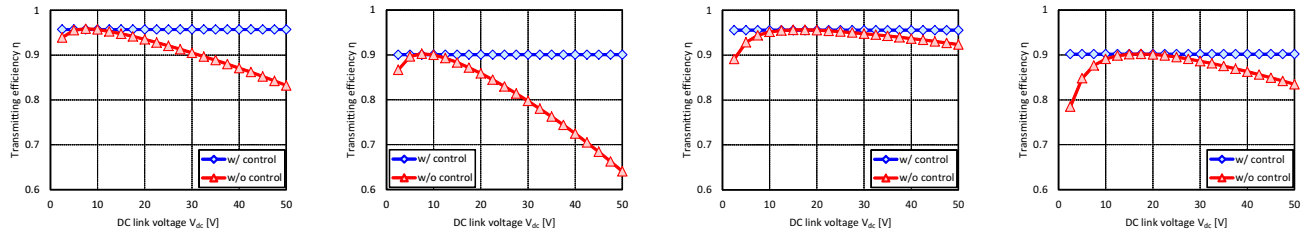

(a) $V_1 = 10$ V, $L_m = 77.8$ μH. (b) $V_1 = 10$ V, $L_m = 37.3$ μH. (c) $V_1 = 20$ V, $L_m = 77.8$ μH. (d) $V_1 = 20$ V, $L_m = 37.3$ μH.

Fig. 13. Experimental results of efficiency maximization using calculated reference voltage.

[6] A. Kurs, A. Karalis, R. Moffatt, J. D. Joannopoulos, P. Fisher, and M. Soljacic, "Wireless power transfer via strongly coupled magnetic resonance," *Science Express on 7 June 2007*, vol. 317, no. 5834, pp. 83–86, Jun. 2007.

[7] M. Kato, T. Imura, and Y. Hori, "Study on maximize efficiency by secondary side control using DC-DC converter in wireless power transfer via magnetic resonant coupling," in *Proc. EVS27*, 2013, pp. 1–5.

[8] T. Imura and Y. Hori, "Maximizing air gap and efficiency of magnetic resonant coupling for wireless power transfer using equivalent circuit and Neumann formula," *IEEE Trans. Ind. Electron.*, vol. 58, no. 10, pp. 4746–4752, Oct. 2011.

[9] M. Kato, T. Imura, and Y. Hori, "New characteristics analysis considering transmission distance and load variation in wireless power transfer via magnetic resonant coupling," in *Proc. IEEE INTELEC*, 2012, pp. 1–5.

[10] T. Hiramatsu, X. Huang, M. Kato, T. Imura, and Y. Hori, "Wireless charging power control for HESS through receiver side voltage control," in *Proc. IEEE APEC*, 2015, pp. 1614–1619.

[11] K. Hata, T. Imura, and Y. Hori, "Simultaneous estimation of primary voltage and mutual inductance based on secondary-side information in wireless power transfer systems," in *Proc. IEEE/MTT-S WPTC*, 2016, pp. 1–3.

[12] T. Ohira, "What in the world is Q?," *IEEE Microw. Mag.*, vol. 17, no.6, pp. 42–49, May 2016.